Chemical Science

EDGE ARTICLE

View Article Online
View Journal | View Issue

Cite this: *Chem. Sci.*, 2016, 7, 5945

Correlating drug–target kinetics and *in vivo* pharmacodynamics: long residence time inhibitors of the FabI enoyl-ACP reductase†

Fereidoon Daryaee,‡[a] Andrew Chang,‡[a] Johannes Schiebel,§[ce] Yang Lu,[a] Zhuo Zhang,[a] Kanishk Kapilashrami,[a] Stephen G. Walker,[b] Caroline Kisker,[c] Christoph A. Sotriffer,[e] Stewart L. Fisher*[d] and Peter J. Tonge*[a]

Received 3rd March 2016
Accepted 20th May 2016

DOI: 10.1039/c6sc01000h

www.rsc.org/chemicalscience

Drug–target kinetics enable time-dependent changes in target engagement to be quantified as a function of drug concentration. When coupled to drug pharmacokinetics (PK), drug–target kinetics can thus be used to predict *in vivo* pharmacodynamics (PD). Previously we described a mechanistic PK/PD model that successfully predicted the antibacterial activity of an LpxC inhibitor in a model of *Pseudomonas aeruginosa* infection. In the present work we demonstrate that the same approach can be used to predict the *in vivo* activity of an enoyl-ACP reductase (FabI) inhibitor in a model of methicillin-resistant *Staphylococcus aureus* (MRSA) infection. This is significant because the LpxC inhibitors are cidal, whereas the FabI inhibitors are static. In addition *P. aeruginosa* is a Gram-negative organism whereas MRSA is Gram-positive. Thus this study supports the general applicability of our modeling approach across antibacterial space.

Introduction

Despite advances in genomics and bioinformatics that have identified a large number of novel drug targets across disease space,[1,2] target-based strategies have resulted in very few new drugs.[3–5] Barriers to success include the growing realization that genetic essentiality does not necessarily equate to druggability, and thus not all essential proteins are actually good targets for drug discovery. In addition, the lack of success suggests that our ability to predict efficacy and selectivity in humans at early stages of drug discovery is inadequate, highlighting the need for improved methods for correlating *in vitro* and *in vivo* measurements of drug activity. In the present work we demonstrate that the integration of drug–target kinetics into a mechanistic mathematical model that links drug pharmacokinetics (PK) and *in vitro* antibacterial activity can be used to predict *in vivo* drug efficacy (PD).

Traditionally, the selection and optimization of drug leads is heavily reliant on thermodynamic parameters such as IC_{50} and K_d values. However, these equilibrium parameters are insufficient to predict efficacy and selectivity in the dynamic *in vivo* environment where drug and target are not at equilibrium.[6–11] As a consequence, drug–target residence time ($t_R = 1/k_{off}$) has emerged as a key parameter in lead optimization in which kinetic parameters are used to drive drug discovery.[7,8,11] This strategy exploits rapid *in vivo* clearance to achieve efficacy and selectivity *via* prolonged dissociation rates from the drug target.

We have developed a mechanistic PK/PD model which is capable of predicting *in vivo* efficacy based on *in vitro* drug–target kinetic parameters.[12] This model successfully predicted the antibacterial activity of a *Pseudomonas aeruginosa* LpxC (*pa*LpxC) inhibitor in a mouse model of infection. To evaluate the generality of our approach, we have now used the model to analyze the antibacterial activity of inhibitors that target the enoyl-ACP reductase (FabI) enzyme in the Gram-positive bacterium *Staphylococcus aureus* (*sa*FabI).[13–15] The *sa*FabI-inhibitors are static inhibitors of *S. aureus* growth in contrast to the *pa*LpxC-inhibitors which display cidal activity against the Gram-negative pathogen *P. aeruginosa*. However, despite these major differences in mechanism and organism, the model is able to fit the time-dependent antibacterial activity of a series of *sa*FabI inhibitors at the cellular level, and also to simulate the efficacy of two selected FabI inhibitors in an animal infection

[a]*Institute for Chemical Biology & Drug Discovery, Department of Chemistry, Stony Brook University, Stony Brook, NY 11794-3400, USA. E-mail: stewfisher@slfisherconsulting.com; peter.tonge@stonybrook.edu*

[b]*Institute for Chemical Biology & Drug Discovery, Department of Oral Biology and Pathology, Stony Brook University, Stony Brook, NY 11794-3400, USA*

[c]*Rudolf Virchow Center for Experimental Biomedicine, Institute for Structural Biology, University of Würzburg, D-97080 Würzburg, Germany*

[d]*The Broad Institute, Cambridge, MA 02142, USA*

[e]*Institute of Pharmacy and Food Chemistry, University of Würzburg, D-97074 Würzburg, Germany*

† Electronic supplementary information (ESI) available: Derivation of PK/PD models. See DOI: 10.1039/c6sc01000h

‡ These authors contributed equally to this work.

§ Present address: Institute of Pharmaceutical Chemistry, Philipps-Universität Marburg, Marbacher Weg 6, D-35032 Marburg, Germany.

model. By comparing the relationship between target inhibition and activity in these two different systems, we are able to gain insight into target vulnerability, which characterizes the degree of inhibition required to elicit the desired pharmacodynamic (PD) response.[16,17]

Results

Long residence time inhibitors of *sa*FabI

To evaluate the applicability of the PK/PD model described previously to other systems,[12] we have now used the model to analyze the *in vitro* and *in vivo* activity of inhibitors of the *S. aureus* FabI enzyme (*sa*FabI) from the bacterial type II fatty acid biosynthesis pathway. Our *sa*FabI inhibitor program has generated several series of compounds including those based on the diphenyl ether scaffold that are time-dependent enzyme inhibitors, a selection of which have excellent *in vitro* activity and efficacy in animal models of infection. For the purposes of this work, we selected four compounds, **PT55**, **PT447**, **PT119** and **SKTS1** with a wide range of residence-times (Fig. 1 and Table 1). **PT119**, **PT55** and **PT447** have been described previously.[18,19] **SKTS1** was designed to explore a hitherto unaddressed region of the binding pocket with the ultimate goal of further increasing affinity and residence time. The binding mode obtained by docking suggests new interactions with Ala97 mediated by nearly ideal hydrogen bonds (Fig. 2). Since **SKTS1** had a predicted IC_{50} of 1 nM, which is ~200-fold lower than the corresponding value for the parent molecule 5-hexyl-2-phenoxyphenol (yellow portion of **SKTS1** in Fig. 2), we selected this molecule for synthesis and further investigation.

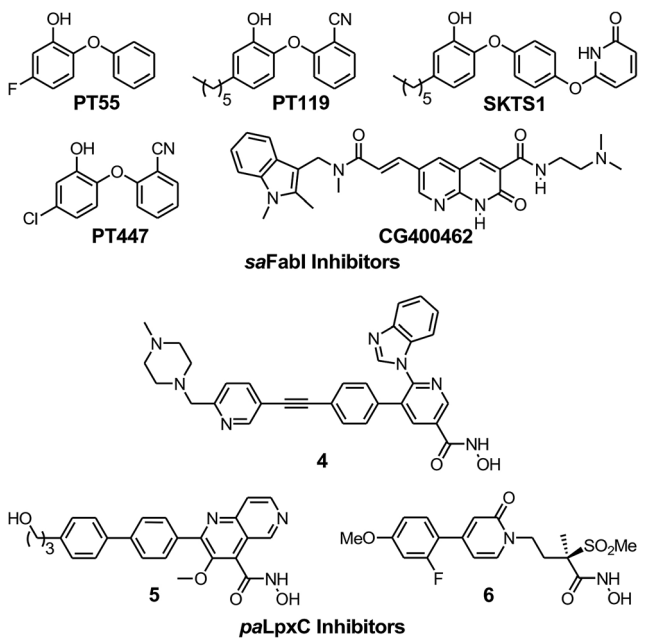

Fig. 1 The *sa*FabI and *pa*LpxC inhibitors used in this work. The *sa*FabI inhibitors **PT55**, **PT119** and **PT447** have been described in Chang *et al.*[18] and Wang *et al.*,[19] and the *pa*LpxC inhibitors in Walkup *et al.*[12] **SKTS1** is described in the present work.

Table 1 Kinetic and cellular parameters for inhibitors of *sa*FabI

Inhibitor	K_i^{app} (nM)	MIC (μM)	t_R (h) 37 °C	PAE[a] (h) 37 °C
PT55	1970	39	0.04	0.25 ± 0.21
PT447	114	8	0.5	0.91 ± 0.11
PT119	89	2	1.78	1.03 ± 0.17
SKTS1	46	10	5.75	2.04 ± 0.18

[a] Post-antibiotic effect (PAE) values are reported at 4x MIC.

K_i^{app} values were determined by progress curve analysis followed by global fitting of the data to eqn (1)–(4). All four compounds showed one-step inhibition (Scheme 1), consistent with previous reports for this series of inhibitors.[18] The dissociation rate constants were then determined at 37 °C using a jump dilution assay, in which the compounds were incubated overnight with *sa*FabI at a concentration above their K_i values, after which reaction mixtures were diluted 1000-fold into the reaction buffer containing excess substrate. This approach yielded residence times of 0.04, 0.5, 1.78 and 5.75 h for **PT55**, **PT447**, **PT119** and **SKTS1**, respectively. In Table 1 it can also be seen that K_i^{app} decreases ~40-fold as residence time increases 140-fold, and thus the increase in the life-time of the drug–target complex results primarily from ground state stabilization in addition to a modest change in transition state stability.[18]

In vitro PAE data analysis: correlation between PAE and t_R

We next determined the time-dependent antibacterial activity of each *sa*FabI inhibitor at the whole cell level by measuring the post-antibiotic effect (PAE), which is the persistent suppression of bacterial growth following antibiotic wash-out.[20] In each case, a longer PAE was observed as the drug concentration increased except for **SKTS1** where the PAE reached a maximum at 4x MIC. **PT55**, a *sa*FabI inhibitor with a very short residence time (0.04 h) had the shortest PAE (0.25 h), whilst the PAE increased with

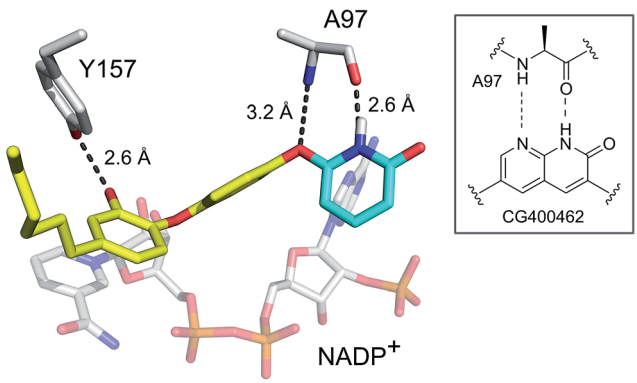

Fig. 2 Rational design of **SKTS1**. The putative binding mode of **SKTS1** derived from our docking study is shown within the *sa*FabI protein structure (selected residues and the cofactor are depicted as gray sticks). The diphenyl ether scaffold of **SKTS1** is indicated in yellow while the novel 6-hydroxypyridin-2(1*H*)-one modification is highlighted in cyan. The inset highlights the underlying concept that drove the design of **SKTS1**.

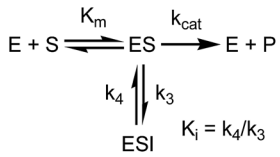

Scheme 1 *sa*FabI inhibition.

residence time for the other compounds (Table 1). The relationship between PAE and residence time (t_R) is shown graphically in Fig. 3, where we also present data for the *pa*LpxC inhibitors reported previously.[12] In each case a positive slope is observed, indicating that prolonged antibacterial activity at low drug concentration is coupled to the life-time of the drug–target complex. In contrast, no correlation was observed between MIC and residence time.

In vitro PAE data analysis: PK/PD model fitting

In order to integrate drug–target kinetics into predictions of *in vivo* drug activity, we previously derived a PK/PD model in which time-dependent changes in target engagement are directly related to inhibition of bacterial growth.[12] This model had to be modified slightly for use with the *sa*FabI inhibitors which follow an uncompetitive one-step mechanism in contrast to the *pa*LpxC inhibitors which bind to their target *via* a competitive two-step mechanism. The derivation of the PK/PD model is outlined in the Methods section (eqn (5)) and described in detail in the ESI (eqn (S14)†).

$$[N] = [N_0]\exp\left(\left[\lambda - \varepsilon\left(1 - \frac{k_4}{\beta k}\right)\right]t + \varepsilon\frac{\left([\mathrm{ES}]_0 - \frac{k_4}{\beta k}\right)}{k}\left(1 - \mathrm{e}^{-kt}\right)\right) \quad \text{(eqn 5 S14)}$$

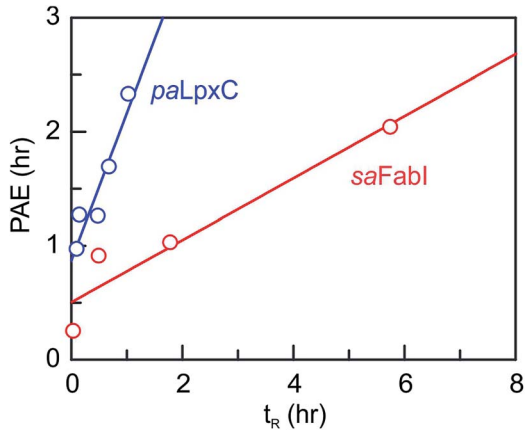

Fig. 3 Correlation between residence time (t_R) and post-antibiotic effect (PAE). Data for *pa*LpxC inhibitors (blue) are from ref. 12. The PAE and t_R values were determined at 37 °C and the PAE values obtained at 4x MIC have been plotted. In each case the data have been fit to a straight line with slope values of 0.27 (*sa*FabI) and 1.3 (*pa*LpxC).

Eqn (5) relates the bacterial cell count ([*N*], CFU mL^{-1}) to the rate of logarithmic cell growth (λ) minus the maximum rate of inhibitor-induced cell death (ε) multiplied by a factor that integrates time-dependent changes in the amount of the enzyme forms that cannot sustain growth ([E] and [EI] in Scheme 1). In eqn (5), k_4 is the rate constant for breakdown of the enzyme-inhibitor complex (ESI†), $\beta = 1 + K_m/[S]$, where $M = K_m/[S]$, and κ is a more complex function that includes the concentration of inhibitor (drug) ([I]) at the target as well as the thermodynamic affinity of the inhibitor for the enzyme (K_i in Scheme 1). Since the intracellular drug concentration is not known, we use a permeability factor (p_m) to relate the concentration of drug in the media (or the free fraction drug concentration in plasma) to the intracellular drug concentration.

In order to use eqn (5) for predictions of *in vivo* drug activity, we first fit the PAE data using the equation to obtain values for M and p_m. The progress curve kinetics (Table 1) yield a seed value for k_4 and a value for the apparent K_i (K_i^{app}) which was used as input for K_i. λ (k_{growth}) was an experimental value and ε ($k_{killmax}$) was assumed to be similar to λ since the *sa*FabI inhibitors are static. Finally, M was assigned a value of unity given the general assumption that the substrate concentration is usually around the value of K_m. Non-linear regression was used to perform global fits of data to the PK/PD model, and excellent fits to the experimental data were obtained (Fig. 4) with the output parameters showing only small changes from the input seed values (Table 2), thus validating the ability of the model to correlate *sa*FabI inhibition with *in vitro* antibacterial activity.

Predicting *in vivo* efficacy of PT55 and PT119 using the mechanistic PD model

The mechanistic PK/PD model was then used to predict the *in vivo* activity of two compounds, **PT55** and **PT119**, that differ significantly in their residence times on *sa*FabI (0.04 and 1.78 h, respectively). The pharmacokinetic (PK) parameters of these compounds in mice were calculated after the administration of a 40 or 100 mg kg^{-1} dose of each compound and the use of a single-compartmental PK model (Table 3). The pharmacodynamic activity of each compound was also evaluated after administration of a single dose (40 mg kg^{-1} or 100 mg kg^{-1}) to mice infected with MRSA by collecting the infected thighs at different time points and plating on Mueller Hinton II agar containing 5% sheep blood. The free fraction of each drug at multiple time-points was then used as input for the PK/PD model to predict drug efficacy. Importantly, this approach was able to replicate the observed change in bacterial load following administration of both drugs (Table 4 and Fig. 5).

Minimum and maximum target occupancy required for antibacterial activity

To estimate TO_{min} and TO_{max} we added a slope function to the PK/PD model in Mathematica. Subsequently, the parameters resulting from global fitting to the original PK/PD model were used as inputs for this new model. We analyzed three of the

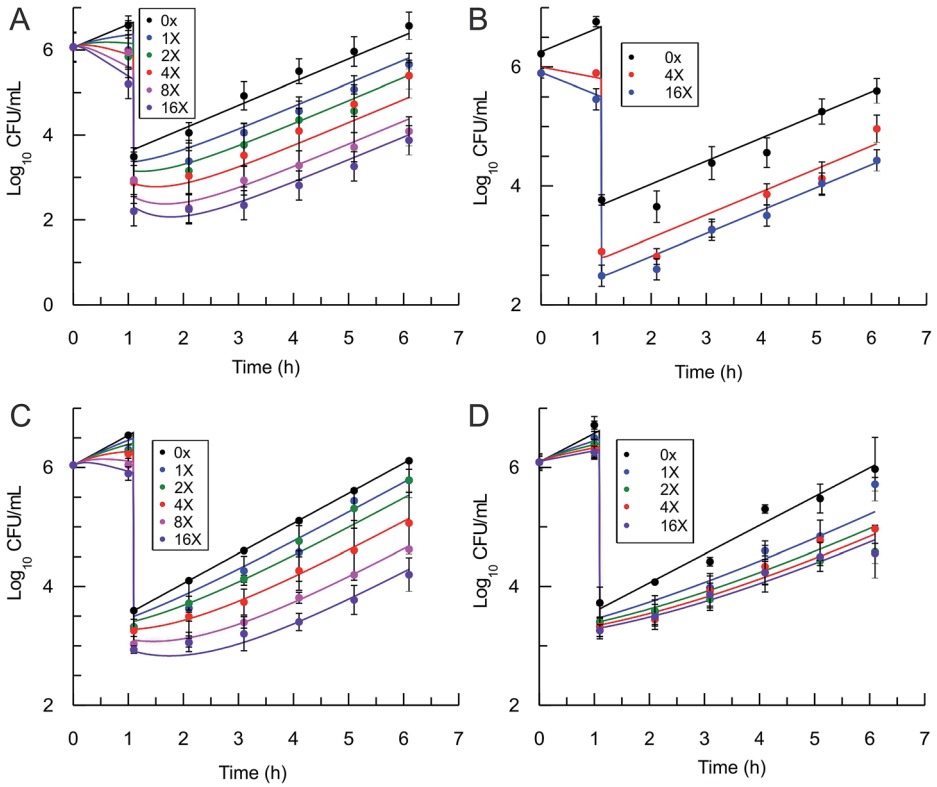

Fig. 4 Post-antibiotic effect of the *sa*FabI inhibitors against *S. aureus*. The recovery of bacterial growth after 1 h exposure and compound washout was measured at various concentrations of inhibitor up to 16x MIC. Experimental data points represent mean values from triplicate, independent measurements and error bars represent 1 s.d. of the $\log_{10}$ CFU mean. Solid lines are the result of global fitting to the PK/PD model (Table 2). A: **PT119**, B: **PT55**, C: **PT447**, D: **SKTS1**.

*sa*FabI inhibitors described in this work and three *pa*LpxC inhibitors reported previously (Table 5).[12] The resulting relationship between target occupancy and antibacterial activity for these two systems has been plotted in Fig. 6 where it can be seen that lower values of *pa*LpxC occupancy are required for activity (TO_{min} 29%, TO_{max} 48%) compared to *sa*FabI (TO_{min} 39%, TO_{max} 76%). Thus *pa*LpxC, is more vulnerable than *sa*FabI consistent with the correlation between drug–target residence time and PAE in both systems (Fig. 3).

Discussion

The ultimate goal of target-based drug discovery is the prediction of *in vivo* efficacy from early *in vitro* parameters. In theory, a kinetics-driven approach works in tandem with the dynamic *in vivo* environment, circumventing the traditional requirement for a stable pharmacokinetic profile by relying on drug–target kinetics to attain prolonged efficacy.[7,8,11] We believe that the kinetics-based approach to drug discovery provides several key

Table 2 *In vitro* PAE model fitting: input and output parameters for **PT119**, **PT55**, **PT447** and **SKTS1**

	PT119			**PT55**			**PT447**			**SKTS1**		
Parameter	Input value	Output value	Ratio	Input value	Output value	Ratio	Input value	Output value	Ratio	Input value	Output value	Ratio
k_4 (min^{-1})	0.009	0.016	1.8	0.43	0.36	0.8	0.033	0.017	0.5	0.0033	0.0038	1.2
λ (k_{growth}) ($\log_{10}$ h^{-1})	1.2	1.2	1.0	1.2	1.2	1.0	1.2	1.2	1.0	1.0	1.1	1.1
ε ($k_{killmax}$) ($\log_{10}$ h^{-1})[a]	1.8	2.1	1.2	1.8	1.8	1.0	1.6	1.7	1.5	1.0	0.9	0.8
K_i^{app} (μM)	0.089	0.098	1.1	1.97	1.81	0.92	0.11	0.17	0.74	0.05	0.04	0.74
p_m/K_i^{app} (μM^{-1})[b]	0.05	0.041	0.82	0.05	0.017	0.3	0.05	0.01	0.2	0.05	0.059	1.2
$M([S]/K_m)$	1.0	0.45	0.45	1.0	0.88	0.88	1.0	0.80	0.80	1.0	1.82	1.8
R^2	0.95			0.97			0.97			0.98		

[a] The *sa*FabI inhibitors are bacteriostatic agents *in vitro* and thus the value of $k_{killmax}$ is similar to the bacterial growth rate (k_{growth}). [b] The input value for p_m/K_i has been chosen randomly within a large constraint range (1/100–100).

Table 3 Pharmacokinetic parameters for **PT55** and **PT119** in mice[a]

In vivo	Volume of distribution (V_d), L kg^{-1}	Clearance (CL), L h^{-1} kg^{-1}	Half-life ($T_{1/2}$), h	Absorption rate (k_a), h^{-1}	AUC/MIC (h μg mL^{-1})/(μg mL^{-1})	t_{max} (h)	C_{max} (ng mL^{-1})
PT55 100 mg kg^{-1}	33 ± 13	20	1.3 ± 0.7	3.5 ± 2.5	0.5	0.75	1200 ± 1100
PT119 100 mg kg^{-1}	40 ± 12	7.4	3.8 ± 2.4	1.7 ± 1.0	9.4	1	760 ± 540
PT119 40 mg kg^{-1}[b]	96	10.8	6.2	0.77	3.5	4	280

[a] *In vitro* data: **PT55**, free fraction of drug (fu) = 0.05, clog P = 3.24; **PT119**, fu = 0.01, clog P = 5.44. [b] From Wang *et al.*[19]

advantages. First, the pharmacokinetic exposure requirement for efficacy is governed by multiple factors which can be easily measured using *in vitro* assays (t_R, K_i), thus providing a more robust set of parameters for lead optimization than traditional methods that rely on thermodynamic measures alone. Second, there is a suggestion that prolonged target binding results in a higher barrier to resistance.[7,21] This would also apply to efflux-mediated resistance, which is particularly relevant in difficult Gram-negative pathogens.[4] Third, the kinetics-driven approach has the potential to improve therapeutic indices by maximizing target engagement using minimal compound exposure. Selectivity can be achieved between similarly potent on- and off-targets *via* modulation of the transition-state barrier.

To provide an experimental framework for evaluating the relevance of drug–target kinetics to *in vivo* drug activity, we previously described a mechanistic PK/PD model that coupled *in vitro* kinetic measurements of drug–target binding with drug PK to predict drug PD. This approach was able to model the *in vitro* PAE for a series of *pa*LpxC inhibitors and to predict the activity of one of these inhibitors in a mouse model of *P. aeruginosa* infection.[12] LpxC catalyzes the first committed step in the biosynthesis of lipopolysaccharide, an essential component of the Gram-negative bacterial cell wall. To evaluate the ability of this model to predict drug activity in other systems, we chose to study inhibitors of the FabI enzyme in the Gram-positive bacterium *S. aureus*. FabI is a component of the bacterial type II fatty acid biosynthesis pathway, and inhibitors of *sa*FabI have a static effect on bacterial growth in contrast to the *pa*LpxC inhibitors which are cidal. The *pa*LpxC inhibitors show a correlation between residence time on the enzyme and the magnitude of the PAE observed following compound washout.[12] Thus we first selected several *sa*FabI inhibitors with a range of residence times, and determined the drug–target kinetic parameters and PAE values at 37 °C (Table 1). As observed in the LpxC system, the PAE resulting from the *sa*FabI inhibitors increases as residence time increases, indicating that prolonged antibacterial activity at low drug concentration is coupled to the life-time of the drug–target complex. However, in Fig. 3 it can be seen that a steeper correlation exists between residence-time and PAE for the *pa*LpxC inhibitors (slope 1.3) compared to that of *sa*FabI inhibitors (slope 0.27), indicating that drug–target residence time in the LpxC system is translated more strongly to the time-dependent efficacy than in the FabI system.

The molecular factors that control the coupling between extended target engagement and time-dependent drug activity play a direct role in determining the sensitivity of a specific target to intervention. In this regard, the rate of protein synthesis will play a key role since the production of new target will dilute the impact of extended target engagement at low drug concentration,[22] and Narberhaus *et al.* have reported that *pa*LpxC is highly stable and thus turns over relatively slowly in *P. aeruginosa*.[23] In addition, the LpxC inhibitors are cidal whereas the FabI inhibitors are static, and growth recovery after exposure to cidal drugs is expected to depend on both the rate of drug–target dissociation and the rate of recovery from downstream events resulting from target engagement. As a result, the PAE depends on both the duration of drug–target interaction as well as the time required for physiological recovery of the process(es) involved in the cidality response. In contrast, static agents are envisioned to induce a dormant growth state, and therefore recovery in this case is anticipated to be primarily dependent upon the rate of drug–target dissociation.

Table 4 *In vivo* efficacy model fitting: input and output parameters for **PT55** and **PT119**

Parameter	**PT55** Input value	**PT55** Output value	**PT55** Ratio	**PT119** Input value	**PT119** Output value	**PT119** Ratio
k_4 (min^{-1})	0.42	0.42	1.0	0.009	0.022	2.4
λ (k_{growth})[a] (log$_{10}$ h^{-1})	0.37	0.73	2.0	0.37	0.66	1.8
ε ($k_{killmax}$) (log$_{10}$ h^{-1})	1.2	1.5	1.2	1.2	1.67	1.4
K_i^{app} (μM)	1.97	1.97	1.0	0.089	0.18	2.0
p_m/K_i (μM^{-1})[b]	0.01	0.04	4.0	0.01	0.001	0.1
$M(K_m/[S])$	1	0.2	0.2	1	0.1	0.1
R^2	0.99			0.98		

[a] The bacterial growth rate (k_{growth}) is assumed to be ~3-fold lower that that observed for *in vitro* growth conditions which most likely reflects nutrient limitation *in vivo*.[12] [b] The input value for p_m/K_i has been chosen randomly within a large constraint range (1/100–100).

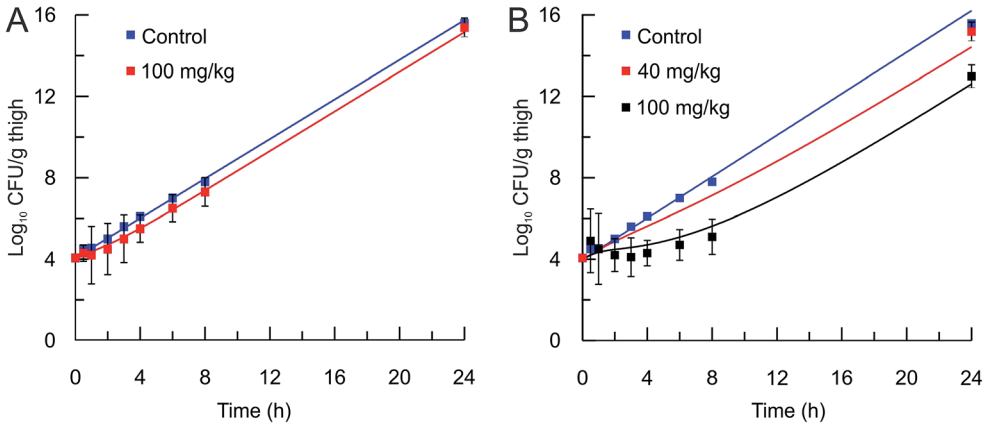

Fig. 5 *In vivo* efficacy and pharmacodynamic modeling of **PT55** and **PT119**. *In vivo S. aureus* MRSA BAA 1762 CFU thigh tissue burden after a single sc dose of the vehicle (blue square) or (A) **PT55** at 100 mg kg^{-1} (red square) or (B) **PT119** at 40 mg kg^{-1} (red squares), or **PT119** at 100 mg kg^{-1} (black squares). Solid lines represent the mechanistic PD simulations using the biochemical parameters from Table 2 and the PK parameters from Table 3. Note that the 40 mg kg^{-1} data set is an efficacy study and only one time point was collected.

Table 5 Minimum (TO_{min}) and maximum (TO_{max}) values of target occupancy of the *sa*FabI and *pa*LpxC inhibitors[a]

	PT447		**PT119**			**SKTS1**	
*sa*FabI	16x	4x	16x	8x	4x	4x	Average
TO_{min}	0.43	0.42	0.33	0.33	0.33	0.49	0.39 ± 0.07
TO_{max}	0.78	0.8	0.68	0.72	0.71	0.84	0.76 ± 0.06
	4		**5**		**6**		
*pa*LpxC	4x	8x	4x	16x	4x	16x	Average
TO_{min}	0.20	0.17	0.27	0.36	0.38	0.36	0.29 ± 0.09
TO_{max}	0.50	0.48	0.50	0.43	0.48	0.48	0.48 ± 0.03

[a] The output parameters from PK/PD modeling of the *sa*FabI inhibitors **PT119**, **PT447** and **SKTS1** (Table 2) and of the *pa*LpxC inhibitors **4–6**,[12] were used as input for the TO PK/PD model to fit the PAE phase for each compound at specific inhibitor concentrations. The average values of TO_{min} and TO_{max} for all the inhibitors of each target were used to generate the plot shown in Fig. 5.

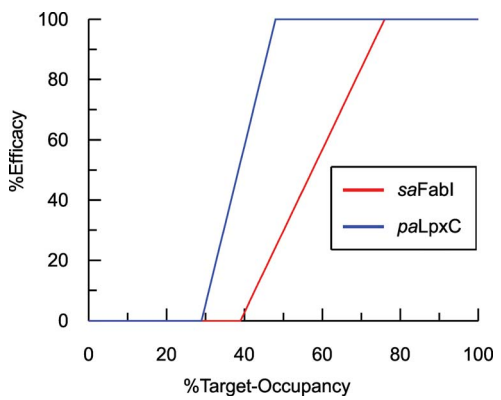

Fig. 6 Correlation between target-occupancy and efficacy for the *sa*FabI and *pa*LpxC inhibitors.

The slope of the t_R PAE correlation is an indication of the vulnerability of each target to engagement – and thus LpxC is a more vulnerable target than FabI under the *in vitro* growth conditions employed for determining the PAE values. It is also possible to access a more quantitative assessment of target vulnerability by using the model fitting to estimate the minimum and maximum levels of engagement that provide the thresholds for the observed antibacterial activity. As demonstrated in the *in vitro* PAE measurements, higher concentrations of drug, expressed as fold-MIC, normally result in longer PAEs. This relationship exists because increased drug concentration leads to higher levels of target-occupancy, and that the time required for recovery from the effect of target engagement is longer at higher levels of occupancy. Although global fitting to the PK/PD model calculates the relative target-occupancies at each drug concentration, this process does not explicitly generate the target-occupancy at each drug concentration at the end of the exposure time, nor the minimum and maximum target-occupancy (TO_{min} and TO_{max}, respectively) that set the threshold limits for the correlation between target occupancy and efficacy which is hypothesized to be linear. This modeling exercise is analogous to the normal sigmoidal correlation that is assumed to exist between drug concentration and effect, where the central section of the sigmoidal curve, which has the largest slope, is approximately linear.[24,25] All non-mechanistic traditional PK/PD models use the Hill equation to predict drug efficacy based on the drug concentration at the site of activity.[24,26–28] According to this logic, a similar sigmoidal relationship is expected to exist between target-occupancy and drug efficacy.

Estimates of TO_{min} and TO_{max} were obtained for inhibitors of *sa*FabI and *pa*LpxC at individual compound concentrations (Table 5). The average values for the TO_{min} and TO_{max} values for all the inhibitors of each enzyme are plotted in Fig. 6 where it can be seen that values for both TO_{min} and TO_{max} are lower for *pa*LpxC compared to *sa*FabI, demonstrating that *pa*LpxC is a more vulnerable target than *sa*FabI. Classification of target

vulnerability in the early stages of the drug development pipeline, based on drug–target binding kinetics and PAE measurements, is likely to reduce the rate of attrition in clinical trials and is also likely to provide valuable information for developing suitable dosing strategies. Specifically, for those drugs that interact with a non-vulnerable target or that have a short residence-time, high concentrations of drug will have to be maintained thus reducing the safety window. Conversely, drugs that target vulnerable targets and also have a long residence time, can be dosed less frequently leading to an increase in the therapeutic window. We note, however, that this vulnerability analysis has been conducted based on antibacterial activity measured in culture. While valuable, it is important to note that a similar correlation developed using *in vivo* efficacy data would be significantly more appropriate since growth conditions, including pressure from the immune system, can alter target vulnerability. In this regard the *sa*FabI inhibitor **PT119** has promising *in vivo* efficacy despite poor bioavailability and high protein binding (>99%), and the conclusion from the *in vitro* data analysis that suggest FabI is a low vulnerability target.

Conclusions

In this report, we have been able to model *in vivo* efficacy data for two *S. aureus* FabI inhibitors using the approach that was used previously for an inhibitor of LpxC.[12] Given the high quality fits of the model to both the FabI and LpxC inhibitors, it is important to note the differences between these two compound series. In addition to targeting very different enzymes and metabolic pathways (FabI, fatty acid biosynthesis; LpxC, cell envelope), the compounds differ in their mode of inhibition (LpxC, competitive inhibition; FabI, uncompetitive inhibition), type of slow-onset inhibition (one-step for FabI and two-step for LpxC inhibition), static time–kill profile (FabI, bacteriostatic; LpxC, bactericidal) and organism that they target (*S. aureus*, Gram-positive; *P. aeruginosa*, Gram-negative). Collectively, these data sets provide a strong argument for the general applicability of the time-dependent pharmacodynamic model.

Experimental

Material and methods

Compounds. The FabI inhibitors **PT119**, **PT55** and **PT447** (Fig. 1) were available from previous studies.[18] **SKTS1** was purchased from COSMIC Discoveries (Hyderabad, India) after commissioned synthesis. Cell growth media (Mueller-Hinton broth/agar and Mueller-Hinton agar + 5% defibrinated sheep blood) and chemicals were obtained from commercial vendors.

Design of SKTS1. The rational design of *sa*FabI inhibitors with improved affinity and/or residence time was based on several structures of the target in complex with $NADP^+$ and different diphenyl ether inhibitors.[18,29] In order to learn which substituents on the diphenyl ether scaffold might improve enzyme-inhibitor interactions, hot-spot analyses of the *sa*FabI binding pocket were performed using the program GRID (version 22, Molecular Discovery, Pinner, United Kingdom) and the knowledge-based DrugScore^X potentials (G. Neudert and G. Klebe, University of Marburg, Germany).[30,31] These studies demonstrated that partially lipophilic moieties contacting the Ala97 carbonyl oxygen with a hydrogen-bond donor might be suitable to extend the diphenyl ether scaffold at the 4′-position. Additionally inspired by comparisons with the ligand CG400462 (ref. 32) (Fig. 1) and a crystal structure of *Bacillus cereus* FabI in complex with a related indole naphthyridinone compound (PDB-code: 3OJF), we postulated that introduction of a 6-hydroxypyridin-2(1*H*)-one group at the 4′-position might lead to favorable interactions with the active site (**SKTS1**). Together with additional candidates for synthesis, **SKTS1** was docked into the *sa*FabI binding pocket using our validated docking protocol as described in Schiebel *et al.*[14,33] Briefly, FlexX (version 3.1.3, BioSolveIT, Sankt Augustin, Germany)[34] was first used to dock **SKTS1** into the available *sa*FabI structures, followed by scoring with DrugScore^X. The putative binding mode and most suitable receptor (in the case of **SKTS1**: PDB-code 4D42) were then selected *via* visual inspection of the top-ranked binding poses. Finally, IC_{50} values were estimated using a FabI-specific empirical scoring function that builds on SFCscore descriptors and was developed specifically for this purpose.[35] **SKTS1** was selected for synthesis due to its high predicted affinity, low log *P* value and reasonable interactions with the protein. Purity of **SKTS1** was confirmed by HPLC and NMR. ^{1}H NMR (400 MHz, acetone-d6) δ ppm 0.87–0.94 (m, 3H), 1.28–1.41 (m, 6H), 1.58–1.68 (m, 2H), 2.55–2.61 (m, 2H), 6.35 (dd, J = 13.87, 7.84 Hz, 2H), 6.73 (dd, J = 8.16, 2.01 Hz, 1H), 6.89–6.95 (m, 4H), 7.06 (d, J = 9.16 Hz, 2H), 7.64 (t, J = 7.91 Hz, 1H). ESI-MS (*m*/*z*): calculated for $C_{23}H_{24}NO_4$ $[M-H]^-$ 378.2; found 378.1 $[M-H]^-$. High resolution MS (*m*/*z*): calculated for $C_{23}H_{25}NO_4H$ $[M+H]^+$ 380.1856; found 380.1855 $[M+H]^+$; calculated for $C_{23}H_{24}NO_4$ $[M-H]^-$ 378.1711; found 378.1717 $[M-H]^-$.

Bacterial strains. The *Staphylococcus aureus* strains RN4220 and MRSA BAA 1762 were used for the microbiology experiments described below.

Inhibition kinetics. Kinetic assays were performed on a Cary 100 spectrophotometer (Varian) at 37 °C. Reaction velocities were measured by monitoring the oxidation of NADPH to $NADP^+$ at 340 nm (ε = 6220 M^{-1} cm^{-1}). For jump dilution assays, *sa*FabI (10 μM), inhibitors at concentrations above their K_i values (~15 μM) and $NADP^+$ (500 μM) were incubated overnight at 37 °C followed by 1000-fold dilution into the reaction buffer (50 mM potassium phosphate pH 7.5, 150 mM NaCl, 1 M potassium glutamate, 8% glycerol) containing *trans*-2-butenoyl-CoA (1.5 mM) (Sigma, Advent Bio) and NADPH (350 μM). The consumption of NADPH was monitored at 340 nm and the resulting progress curves were fit to eqn (1) using MATLAB 7.0 where v_0 is the initial velocity observed in the presence of inhibitor and v_f is the final velocity following dissociation of the inhibitor and is equal to the uninhibited enzyme velocity (*i.e.* $v_0 < v_f$). Eqn (1) yielded the recovery rate-constant (k_{obs}) from which the residence time was estimated ($t_R \sim 1/k_{obs}$).

$$A_t = A_0 - v_f t + \frac{(v_f - v_0)}{k_{obs}}\left(1 - e^{-k_{obs}t}\right) \quad (1)$$

Analysis of the jump-dilution data using eqn (1) provided an estimate for the residence time which was subsequently used as a seed value for global fitting of the forward progress curve data to eqn (2)–(4). Note that for the forward progress curve analysis using eqn (2), v_0 is the initial velocity observed in the presence of inhibitor and v_s is the steady state velocity in the presence of inhibitor (*i.e.* $v_0 > v_s$). The value of k_{off} was constrained within the limits set by the standard deviation leading to estimates of k_{off} and K_i^{app}.

$$A_t = A_0 - v_s t + \frac{(v_s - v_0)}{k_{obs}}\left(1 - e^{-k_{obs} t}\right) \quad (2)$$

$$\frac{v_s}{v_0} = \frac{1}{\left(1 + \frac{I}{K_i^{app}}\right)} \quad (3)$$

$$k_{obs} = k_{off}\left(\frac{v_0}{v_s}\right) \quad (4)$$

MIC measurements. MIC values were determined with the microbroth dilution assay according to the Clinical and Laboratory Standards Institute methods for antimicrobial susceptibility tests for aerobically growing bacteria.[36]

Post-antibiotic effect (PAE). A starter culture of the antibiotic-sensitive *S. aureus* strain RN4220 was grown to log phase ($OD_{600} = 0.5$; 10^8 CFU mL^{-1}) and diluted 100-fold into cation-adjusted Mueller-Hinton (CAMH) media containing either drug or an equal volume of DMSO. Cultures were then shaken at 37 °C for 1 h after which both treated and untreated cells were diluted 1000-fold in fresh CAMH media and again incubated at 37 °C. Regrowth was monitored by removing aliquots (0.1 mL) of culture at hourly intervals and plating serial dilutions on Mueller-Hinton agar containing sheep blood. The number of CFUs was then counted following overnight incubation of plates at 37 °C. The post-antibiotic effect was calculated as the time in hours required for the number of compound-treated cells (CFUs) to increase 1 $\log_{10}$ above the count immediately after dilution minus the time in hours required for the number of cfu's in the control culture to increase by 1 $\log_{10}$ above the count immediately after the dilution.[20]

Compound pharmacokinetics. Pharmacokinetic (PK) studies were conducted in CD-1 mice *via* subcutaneous (sc) administration of the test agents in a vehicle of 40% H_2O/40% EtOH/20% PEG-400. Plasma samples were collected from animals at eight distinct time points (5 min, 15 min, 30 min, 1 h, 2 h, 4 h, 8 h and 24 h post-injection). Three mice were used per time point.[19] Plasma concentrations for each sample were determined by LC/MS/MS using a calibration curve, and the PK parameters were calculated with WinNonlin (Pharsight Corporation, Mountain View, CA, USA). All animals used in this study were maintained in accordance with the American Association for Accreditation of Laboratory Animal Care criteria. The experimental protocol for both the PK studies and the pharmacodynamics studies (below) was approved by the Institutional Animal Care and Use Committee (IACUC) at Stony Brook University. The animal studies were performed under the protocol "*In vivo* pharmacokinetic and pharmacodynamic evaluation of novel antibacterial agents" (IACUC #383230).

Plasma protein binding. The free fraction of **PT55** and **PT119** in plasma was determined by rapid equilibrium dialysis using a Thermo Scientific™ Single-Use RED Plate. A solution of each compound was prepared in mouse plasma to match the C_{max} determined in the PK study (1.82 μg mL^{-1} for **PT55** and 0.79 μg mL^{-1} for **PT119**). Then 200 μL of each solution was transferred to the plasma chamber of the Thermo Scientific™ Single-Use RED Plate and PBS was placed in the corresponding buffer chamber. The plate was sealed and incubated at 37 °C on an orbital shaker at ~250 rpm for 4 h. Subsequently, the amount of compound in the plasma and buffer samples was determined by LC/MS/MS and the free fraction was calculated by taking the ratio of compound concentration in the buffer and plasma chambers.

Pharmacodynamics. For pharmacodynamic studies, six-week old, specific-pathogen free, male Swiss Webster mice weighing 27 g to 32 g (Taconic) were used. Mice were rendered neutropenic with IP doses of cyclophosphamide (150 mg kg^{-1}, uid), 4 and 1 day before the infection challenge. Infection was induced by injection of *S. aureus*, MRSA (BAA 1762, 10^6 CFU in 50 μL of saline) into the left thigh muscle (IM). Infected neutropenic mice were given a single dose of vehicle or one of the antibacterial agents 1 h post infection by SC injection in the back of the neck. Mice were euthanized by CO_2 inhalation at 24 h (efficacy), or at different time points post infection (*in vivo* PAE). Muscle tissue from the infected thighs was collected, weighed and homogenized in 2 mL of saline. Serial dilutions of each homogenized sample were plated on Mueller Hinton II agar containing 5% difibrinated sheep blood. The bacterial burden per gram of thigh muscle was calculated from the number of viable bacteria following overnight incubation at 37 °C on agar media.[19]

Mechanistic PK/PD model for *sa*FabI inhibition. To minimize complexity we have used the simple inhibition mechanism shown in Scheme 1 to derive the appropriate PK/PD model for inhibition of *sa*FabI. *pa*LpxC is a single substrate enzyme and inhibitors bind to *pa*LpxC through a competitive two-step induced-fit mechanism.[12] In contrast, *sa*FabI catalyzes the NADPH-dependent reduction of an enoyl-ACP substrate through a ternary complex mechanism, and the *sa*FabI inhibitors bind through a one-step mechanism to the E-$NADP^+$ product complex formed during substrate turnover.[18] Thus, the ES complex presented in Scheme 1 represents all *sa*FabI enzyme-complexes capable of binding to the inhibitor. On this basis, we derived a mechanistic PK/PD model (eqn (1), (S14)†) that incorporates one-step uncompetitive inhibition (see ESI†).[12]

$$[N] = [N_0]\exp\left(\left[\lambda - \varepsilon\left(1 - \frac{k_4}{\beta k}\right)\right]t + \varepsilon\frac{\left([ES]_0 - \frac{k_4}{\beta k}\right)}{k}\left(1 - e^{-kt}\right)\right) \quad \text{(eqn 5 S14)}$$

Global fitting of *in vitro* and *in vivo* antibacterial activity. *In vitro* cellular PAE data were obtained at a range of drug concentrations, from 1x MIC to 16x MIC. The PAE data at each drug concentration (three replicates), expressed as CFU mL^{-1} as a function of time, were then globally fit to eqn (5) using initial estimates of the parameters K_i^{app}, k_4, M ($= K_m/[S]$), p_m/K_i, k_{growth} and $k_{killmax}$. The analysis takes the initial inhibitor concentration as an input value which is assumed to remain constant until the dilution step. The program returns fitted values for these parameters as well as an R^2 value.

In vivo time dependent antibacterial activity was simulated using eqn (5) and using the fitted values from the cellular PAE analysis as input values. In this case the input drug concentration as function of time was obtained from the PK analysis.[12]

Estimation of TO_{min} and TO_{max} using a new mechanistic tool. To provide estimates of the minimum (TO_{min}) and maximum (TO_{max}) target occupancy required for antibacterial activity, a slope factor (eqn (6)) was added to the PK/PD models used to analyze the inhibition of paLpxC (Walkup *et al.*)[12] and *sa*FabI (this work) (see ESI eqn (S15)†). TO_{min} is the minimum target occupancy required for activity below which no activity is observed, whereas TO_{max} is the maximum occupancy, above which no further increase in activity is observed. Between TO_{min} and TO_{max} a linear correlation is assumed to exist between occupancy and drug activity.

$$0 < \frac{(1 - [ES]_t) - TO_{min}}{TO_{max} - TO_{min}} < 1 \qquad \text{(eqn 6 S16)}$$

The PAE data sets for the *pa*LpxC inhibitors **4**, **5** and **6** (Fig. 1),[11] and the *sa*FabI inhibitors **PT119**, **PT447** and **SKTS1**, were globally fit to the respective PK/PD models using MATLAB. The resulting output values for the kinetic parameters, k_{growth}, k_{kill} and the permeability factor were used as inputs for the TO PK/PD model. The input values were fixed at their initial values and the change in CFU mL^{-1} as a function of time for the PAE phase was analyzed by the TO PK/PD model in Mathematica to find the best fit for each individual concentration of each compound enabling values of TO_{min}, TO_{max} and the initial value for $[ES]_t$, at the beginning of the PAE phase, to be determined.

Conflict of interest

The authors declare no competing financial interest.

Acknowledgements

This research was funded by NIH/NIGMS (PJT GM102864), and, in part, by the Deutsche Forschungsgemeinschaft DFG (SFB630 to C.A.S and C.K.).

Notes and references

1 D. Becker, M. Selbach, C. Rollenhagen, M. Ballmaier, T. F. Meyer, M. Mann and D. Bumann, *Nature*, 2006, **440**, 303–307.
2 R. Guimera and L. A. Nunes Amaral, *Nature*, 2005, **433**, 895–900.
3 M. N. Gwynn, A. Portnoy, S. F. Rittenhouse and D. J. Payne, *Ann. N. Y. Acad. Sci.*, 2010, **1213**, 5–19.
4 D. J. Payne, M. N. Gwynn, D. J. Holmes and D. L. Pompliano, *Nat. Rev. Drug Discovery*, 2007, **6**, 29–40.
5 C. Walsh, *Nat. Rev. Microbiol.*, 2003, **1**, 65–70.
6 R. A. Copeland, *Future Med. Chem.*, 2011, **3**, 1491–1501.
7 R. A. Copeland, D. L. Pompliano and T. D. Meek, *Nat. Rev. Drug Discovery*, 2006, **5**, 730–739.
8 H. Lu and P. J. Tonge, *Curr. Opin. Chem. Biol.*, 2010, **14**, 467–474.
9 P. J. Tummino and R. A. Copeland, *Biochemistry*, 2008, **47**, 8465.
10 R. Zhang and F. Monsma, *Curr. Opin. Drug Discovery Dev.*, 2009, **12**, 488–496.
11 R. A. Copeland, *Nat. Rev. Drug Discovery*, 2016, **15**, 87–95.
12 G. K. Walkup, Z. You, P. L. Ross, E. K. Allen, F. Daryaee, M. R. Hale, J. O'Donnell, D. E. Ehmann, V. J. Schuck, E. T. Buurman, A. L. Choy, L. Hajec, K. Murphy-Benenato, V. Marone, S. A. Patey, L. A. Grosser, M. Johnstone, S. G. Walker, P. J. Tonge and S. L. Fisher, *Nat. Chem. Biol.*, 2015, **11**, 416–423.
13 H. J. Li, C. T. Lai, P. Pan, W. Yu, N. Liu, G. R. Bommineni, M. Garcia-Diaz, C. Simmerling and P. J. Tonge, *ACS Chem. Biol.*, 2014, **9**, 986–993.
14 J. Schiebel, A. Chang, S. Shah, Y. Lu, L. Liu, P. Pan, M. W. Hirschbeck, M. Tareilus, S. Eltschkner, W. Yu, J. E. Cummings, S. E. Knudson, G. R. Bommineni, S. G. Walker, R. A. Slayden, C. A. Sotriffer, P. J. Tonge and C. Kisker, *J. Biol. Chem.*, 2014, **289**, 15987–16005.
15 P. Pan, S. E. Knudson, G. R. Bommineni, H. J. Li, C. T. Lai, N. Liu, M. Garcia-Diaz, C. Simmerling, S. S. Patil, R. A. Slayden and P. J. Tonge, *ChemMedChem*, 2014, **9**, 776–791.
16 D. Czock and F. Keller, *J. Pharmacokinet. Pharmacodyn.*, 2007, **34**, 727–751.
17 J. Gabrielsson, O. Fjellstrom, J. Ulander, M. Rowley and P. H. Van Der Graaf, *Curr. Top. Med. Chem.*, 2011, **11**, 404–418.
18 A. Chang, J. Schiebel, W. Yu, G. R. Bommineni, P. Pan, M. V. Baxter, A. Khanna, C. A. Sotriffer, C. Kisker and P. J. Tonge, *Biochemistry*, 2013, **52**, 4217–4228.
19 H. Wang, Y. Lu, L. Liu, S. W. Kim, J. M. Hooker, J. S. Fowler and P. J. Tonge, *Eur. J. Med. Chem.*, 2014, **88**, 66–73.
20 R. W. Bundtzen, A. U. Gerber, D. L. Cohn and W. A. Craig, *Rev. Infect. Dis.*, 1981, **3**, 28–37.
21 K. E. Hightower, R. Wang, F. Deanda, B. A. Johns, K. Weaver, Y. Shen, G. H. Tomberlin, H. L. Carter III, T. Broderick, S. Sigethy, T. Seki, M. Kobayashi and M. R. Underwood, *Antimicrob. Agents Chemother.*, 2011, **55**, 4552–4559.
22 A. Lewandowicz, P. C. Tyler, G. B. Evans, R. H. Furneaux and V. L. Schramm, *J. Biol. Chem.*, 2003, **278**, 31465–31468.
23 S. Langklotz, M. Schakermann and F. Narberhaus, *J. Bacteriol.*, 2011, **193**, 1090–1097.
24 R. C. Li, S. W. Lee and C. H. Kong, *J. Antimicrob. Chemother.*, 1997, **40**, 39–45.

25 L. Liu, J. Di Paolo, J. Barbosa, H. Rong, K. Reif and H. Wong, *J. Pharmacol. Exp. Ther.*, 2011, **338**, 154–163.
26 R. C. Li, *Antimicrob. Agents Chemother.*, 1996, **40**, 2306–2310.
27 B. V. de Araujo, A. Diniz, E. C. Palma, C. Buffe and T. Dalla Costa, *J. Antibiot.*, 2011, **64**, 439–446.
28 F. Del Bene, M. Germani, G. De Nicolao, P. Magni, C. E. Re, D. Ballinari and M. Rocchetti, *Cancer Chemother. Pharmacol.*, 2009, **63**, 827–836.
29 J. Schiebel, A. Chang, H. Lu, M. V. Baxter, P. J. Tonge and C. Kisker, *Structure*, 2012, **20**, 802–813.
30 H. F. Velec, H. Gohlke and G. Klebe, *J. Med. Chem.*, 2005, **48**, 6296–6303.
31 P. J. Goodford, *J. Med. Chem.*, 1985, **28**, 849–857.
32 H. S. Park, Y. M. Yoon, S. J. Jung, I. N. Yun, C. M. Kim, J. M. Kim and J. H. Kwak, *Int. J. Antimicrob. Agents*, 2007, **30**, 446–451.
33 J. Schiebel, A. Chang, B. Merget, G. R. Bommineni, W. Yu, L. A. Spagnuolo, M. V. Baxter, M. Tareilus, P. J. Tonge, C. Kisker and C. A. Sotriffer, *Biochemistry*, 2015, **54**, 1943–1955.
34 M. Rarey, B. Kramer, T. Lengauer and G. Klebe, *J. Mol. Biol.*, 1996, **261**, 470–489.
35 C. A. Sotriffer, P. Sanschagrin, H. Matter and G. Klebe, *Proteins*, 2008, **73**, 395–419.
36 F. R. Cockerill, M. A. Wilkler, J. Alder, M. N. Dudley, G. M. Eliopoulos, M. J. Ferraro, D. J. Hardy, J. A. Hindler, J. B. Patel, M. Powell, J. M. Swenson, R. B. Thomson, M. M. Traczewski, J. D. Turnidge, M. P. Weinstein and B. L. Zimmer, *Clinical and Laboratory Standards Institute (CLSI)*, 2012, p. 32.